www.lpr-journal.org

LASER & PHOTONICS REVIEWS

WILEY-VCH

WILEY ONLINE LIBRARY

Early View publication on wileyonlinelibrary.com
(issue and page numbers not yet assigned;
citable using Digital Object Identifier – DOI)

LASER & PHOTONICS REVIEWS

Laser Photonics Rev., 1–6 (2013) / **DOI** 10.1002/lpor.201300123

Abstract A superoscillatory focusing lens has been experimentally demonstrated by optimizing Fresnel zone plates (FZP), with limited physical insight as to how the lens feature contributes to the focal formation. It is therefore imperative to establish a generalized viable account for both FZP (amplitude mask) and binary optics (phase mask). Arbitrary superoscillatory spots can now be customized and realized by a realistic optical device, without using optimization. It is counterintuitively found that high spatial frequency with small amplitude and destructive interference are favorable in superfocusing of a superoscillation pattern. The inevitably high sidelobe is pushed 15λ away from the central subwavelength spot, resulting in significantly enlarged field of view for viable imaging applications. This work therefore not only reveals the explicit physical role of any given metallic/dielectric rings but also provides an alternative design roadmap of superresolution imaging. The robust method is readily applicable in superthin longitudinally polarized needle light, quantum physics and information theory.

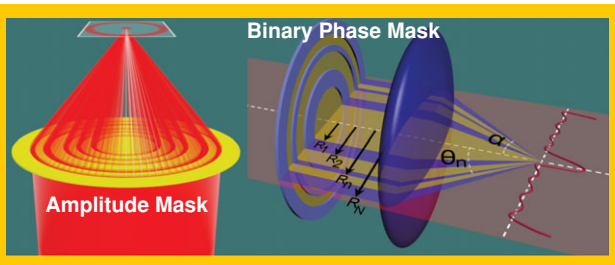

ORIGINAL PAPER

Optimization-free superoscillatory lens using phase and amplitude masks

Kun Huang[1], Huapeng Ye[1], Jinghua Teng[2], Swee Ping Yeo[1], Boris Luk'yanchuk[3], and Cheng-Wei Qiu[1,*]

To observe microscale objects, people always pursue superresolution imaging by decreasing the focused spot [1], tailoring the evanescent wave [2, 3], utilizing the nonlinear effect [4], exploiting the digital-image-processing technique [5, 6] and developing novel equipments [7, 8]. The newly demonstrated optical microscopy based on superoscillatory focusing provides another route to superresolution imaging [9]. This superoscillatory optical microscopy with the resolution of λ/6 has gained much attention because its focused spot can be infinitesimally sharp according to the superoscillation theory, which opens up a promising conceptual avenue to imaging arbitrarily small objects. Nevertheless, the superoscillatory spot with smaller feature suffers from its higher sidelobe, which, to some extent, imposes great challenges in the further application in high-resolution imaging resolution. Since the superoscillatory spot is inevitably accompanied by its high sidelobe [10, 11], one cannot eliminate the sidelobe if the superoscillation arises. Hence, it is nontrivial and imperative to push the high sidelobe far enough apart from the center, so as to produce realistic applications. However, this requires the elaborate manipulation over superoscillation via complicated lens design. The reported methods of constructing a superoscillatory pattern in an optical lens mainly rely on optimizing algorithms [9, 12] for FZP. Hence, the underlying physics, relating every feature of the physical lens structure and their contribution on the imaging plane, is not revealed yet, which in turn limits the flexible and controlled design of the superoscillation imaging in not only FZP but also binary-phase masks [13].

It is well known that the superoscillation in optics is one kind of destructive interference of light with different frequencies at some points at small intervals by matching the amplitude of every frequency [14]. This implies that one can control the optical superoscillation by choosing a suitable amplitude and frequency of light for the destructive interference at the prescribed position, which is a prototype inverse problem. We find that this inverse problem in some realistic optical devices, e.g., a zone plate (amplitude mask) or a binary-phase lens system (phase mask), can be described by a nonlinear matrix equation. Solving that can produce a customized superoscillatory pattern or control the superoscillation optionally. In contrast to using optimization for designing multiple rings as the only way, the unveiled fundamental physics behind the matrix enables us to analytically design a superfocusing central spot and push the high sidelobe away from the center for several wavelengths. In addition, we also attempt to propose a superoscillatory criterion in optical focusing, $r_S = 0.38/f_{max}$ (f_{max} is the maximum spatial frequency), which determines whether the superoscillatory focusing occurs or not.

In contrast to the nanohole array [15], the zone plate with the amplitude modulation of 0 or 1 is an easy method to focus light into a superoscillatory spot. Optimization turns out to be the only method reported so far that can optimize the central radius and width of every belt in a

[1] Department of Electrical and Computer Engineering, National University of Singapore, 4 Engineering Drive 3, Singapore 117583, Singapore
[2] Institute of Materials Research and Engineering, Agency for Science, Technology and Research, Singapore 117602, Singapore
[3] Data Storage Institute, Agency for Science, Technology and Research, 5 Engineering Drive 1, Singapore 117608, Singapore
*Correspondence author: e-mail: eleqc@nus.edu.sg

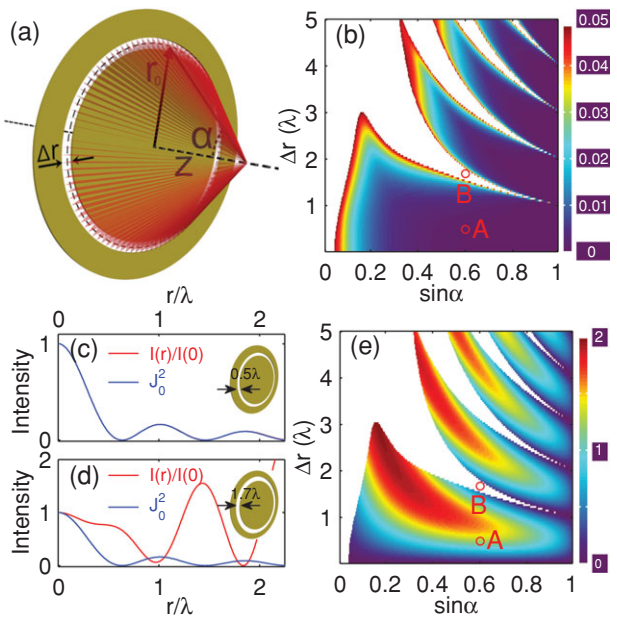

Figure 1 The single belt's diffraction at the intermediate region (where $z = 20\lambda$) between the evanescent (near-field) and far-field region. (a) The optical system describing the diffraction of a single belt with its width Δr and radius r_0. (b) The dependence of RMSE on the width Δr and radius r_0 (or $\sin\alpha$). The smaller the RMSE, the better the approximation between the intensity profile at the target plane and its zero-order Bessel function $|J_0(kr\sin\alpha)|^2$ with the same $\sin\alpha$ ($= r_0/(r_0^2+z^2)^{1/2}$). We just show the cases with small RMSE located in the colored region. The geometry parameters of the single belt are $(\sin\alpha, \Delta r)_A = (0.6, 1.7\lambda)$ at A and $(\sin\alpha, \Delta r)_A = (0.6, 0.5\lambda)$ at B. (c and d) The 1-dimensional intensity profiles (red) of light passing through the belt with its parameters at position A (c) and position B (d) and their corresponding Bessel functions with the same $\sin\alpha$ (blue). The intensity profile in (c) shows an excellent coincidence with the Bessel function so that it is hard to distinguish them. (e) The dependence of the amplitude-modulation coefficient $|C_n|$ in Eq. (1) on the width Δr and radius r_0 (or $\sin\alpha$).

zone plate [9]. Unfortunately, such an optimization-based method presents little physical information but a fitness function containing lens parameters and the designed superoscillatory spot, which is not able to provide an insightful means for controlling the superoscillatory focusing with a customized pattern in the imaging plane, e.g., the peak ratio of sideband over central spot, the distance between high sidelobe and the center. These are actually nontrivial in practical imaging industries, when one wants to use a superoscillatory lens. In this connection, the contribution of our optimization-free design principle for a superoscillatory lens is three-fold: First, the design process is fully guided by the proposed theory; Secondly, the approach applies not only to an amplitude mask but also a phase mask; Thirdly, customization and solving the disadvantage of a superoscillatory lens, i.e. higher sidelobe too close to the central spot.

Figure 1 shows the diffraction of light by a single belt with its geometry of radius r_0 and width Δr, as shown in Fig. 1a. In order to evaluate the focusing properties of a single belt, we use the root-mean-square error (RMSE, whose definition is available in Supplementary Materials) between its diffracting intensity at the target plane and its corresponding zero-order Bessel function of $|J_0(kr\sin\alpha_0)|^2$ with the same $\sin\alpha_0$ ($= r_0/(r_0^2+z^2)^{1/2}$). Figure 1b shows the relationship between RMSE and the geometry (in terms of width Δr and radius r_0) of a single belt. The light from a belt has the different intensity profile at the target plane when the geometry of the transparent belt in Fig. 1a changes. Only the light passing through the belt with its geometry located in the colored region of Fig. 1b has a better focusing pattern with small RMSE, which can be approximated as a zero-order Bessel function of the first kind as shown in Fig. 1c, at the target plane. However, the intensity profile for the case of A in Fig. 1d might destroy the total intensity of the superoscillatory focusing for a subwavelength spot due to its poor focusing property at $r = 0$ and the incomplete destructive interference at its first valley. The optimizing algorithm behaves poorly in rejecting the case of A by itself. In addition, even if all the belts in a zone plate have the geometry located in the colored region, it is still an arduous task for the optimizing method to realize the prescribed intensity (i.e. complete destructive interference with zero intensity) at the customized radial (r) position in the total intensity of the zone plate. To achieve the customized intensity pattern, we here suggest a mathematical method by solving a nonlinear matrix equation, without any optimizing technique involved, to design a superoscillatory mask.

Although some attempts based on the inverse of the matrix have been made to construct a superoscillatory pattern and diffraction-free beam [14, 16, 17], this method is only constrained to the case that the unknown amplitude-modulation coefficients are independent of the spatial frequency. For the zone plate, the amplitude-modulation coefficient from every spatial frequency has a tight relationship, shown in Fig. 1e, with the geometry of the transparent belt in the zone plate, which makes designing of a superoscillatory zone plate very challenging. Here, we develop this method further to design a superoscillatory mask with customized pattern in a realistic optical system. For simplicity, we assume that the illuminated light of the mask is an unpolarized plane wave with uniform distribution in the paper. According to the scalar Rayleigh–Sommerfeld diffraction theory [18], for an unpolarized incident beam passing through the unobstructed belt with radius R_n and width Δr in Fig. 2a, its electric field at the target plane beyond the evanescent region is

$$U_n(r) = \frac{1}{2\pi}\int_{R_n-\Delta r/2}^{R_n+\Delta r/2}\int_0^{2\pi} u(r,\phi)\frac{\partial}{\partial z}\left[\frac{\exp(ikR)}{R}\right]\rho\,\mathrm{d}\rho\,\mathrm{d}\phi, \quad (1)$$

where $R^2 = z^2+r^2+\rho^2-2r\rho\cos(\theta-\varphi)$, the complex amplitude $u(\rho,\varphi)$ of the incident beam is taken as unity for the uniform illumination here. The electric field mainly depends on the R_n, Δr and z. We define the amplitude-modulation coefficient $C_n = U_n(0)$ and the normalized

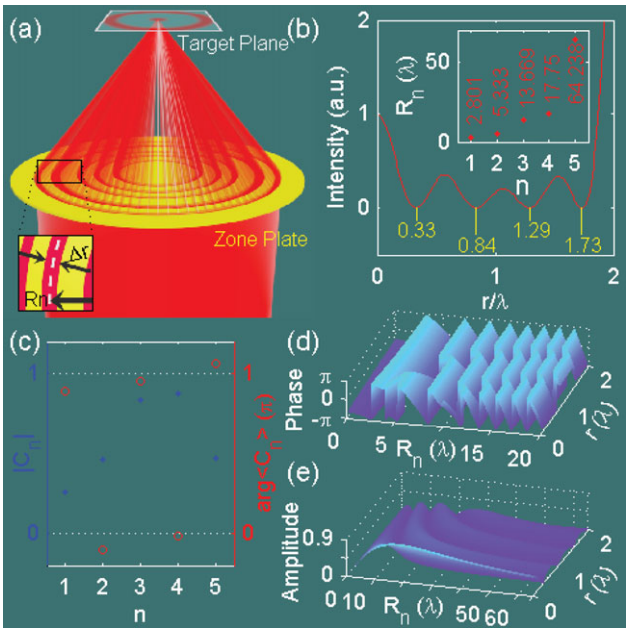

Figure 2 Generation of superoscillatory focusing with the sidelobe away from the center by using a zone plate. (a) The sketch of focusing light beyond the evanescent region by using the zone plate. The *n*th belt in the zone plate has the radius of R_n and width Δd. (b) The constructed optical superoscillatory pattern with the prescribed position $r = [0, 0.33\lambda, 0.84\lambda, 1.29\lambda, 1.73\lambda]$ and the customized intensity $\mathbf{F} = [1, 0, 0, 0, 0]$ at $\mathbf{r}$. Inset: the solved R_n of every belt with fixed $\Delta r = 0.3\lambda$. (c) The modulus (dot) and phase (circle) of the amplitude-modulated coefficient C_n in the solved zone plate of (b). (d and e) The phase (d) and intensity (e) profiles of a belt with its width $\Delta r = 0.3\lambda$ and the changing radius R_n.

amplitude $A_n(r) = U_n(r)/C_n$. Figure 1b shows the root-mean-square error (RMSE) between $|A_n(r)|^2$ and its corresponding zero-order Bessel function of $|J_0(kr\sin\alpha_n)|^2$ with the same $\sin\alpha_n$ ($= R_n/(R_n{}^2+z^2)^{1/2}$). In Fig. 1c, one can see that $|C_n|$ has a strong dependence on the width Δr and the spatial frequency designated as $\sin\alpha/\lambda$. Then, the total electric field of light passing through a zone plate containing N belts can be expressed as

$$U(r) = \sum_{n=1}^{N} C_n A_n(r). \tag{2}$$

To realize the intensity $\mathbf{F} = [f_1, f_2, .., f_M]^T$ at the position $\mathbf{r} = [r_1, r_2, \ldots, r_M]^T$ in the target plane, we can described this problem as

$$\mathbf{SC} = \mathbf{F}, \tag{3}$$

where $\mathbf{S}$ is an $M \times N$ matrix with its matrix element $S_{mn} = A_n(r_m)$ according to Eq. (2) and $\mathbf{C} = [C_1, C_2, \ldots, C_N]^T$, where the sign T means the transpose of matrix. The solution of Eq. (3) exists if $M \leq N$. Here, we just consider the case $M = N$ for which Eq. (3) has the only solution. Because the S_{mn} and C_n are dependent on the unknown R_n (or $\sin\alpha_n$) when the width Δr and z are fixed, it is a nonlinear problem to solve the matrix equation for R_n. Although, in general, Eq. (3) has no analytical solution like the cases in [14, 17], its numerical solution can be easily obtained by using the well-developed Newton's theory, which has been widely used to deal with the nonlinear problem in many areas [19,20]. Newton's theory for nonlinear problems solves Eq. (3) on the basis of the exact solution of its subproblem [20], which makes it a powerful tool to efficiently approach the exact solution without any search-based optimizing algorithm. The method described in Eq. (3) provides a very useful way to design a superoscillatory zone plate despite the fact that the solution is numerically approximated.

To verify the validity of our method, we show a constructed superoscillatory spot with size of about $0.5r_R$ (r_R is the Rayleigh limitation) and its sidelobe is about 1.8λ away from the center by using a zone plate, shown in Fig. 2a, which is designed by our method. In order to realize the goal of pushing away the sidelobe, we pad the zero intensity at the locations between the sidelobe and the center to suppress the high sidelobe near the center. The customized position $\mathbf{r}$ with zero intensity must be carefully chosen to reject the generation of any high intensity between the high sidelobe and the center when solving Eq. (3). Therefore, we choose $\mathbf{F} = [1, 0, 0, 0, 0]^T$ at $\mathbf{r} = [0, 0.33\lambda, 0.84\lambda, 1.29\lambda, 1.73\lambda]^T$ for achieving a superoscillatory spot with the size of $0.5r_R$ (0.33λ) and its sidelobe about 2λ away from the center in Fig. 2b. In the customized $\mathbf{F}$ and $\mathbf{r}$, $f_1 = 1, f_2 = 0$ and $r_1 = 0.33\lambda$ are used to define the superoscillatory spot and the rest is responsible for suppressing the sidelobe between the main spot and the high sidelobe. According to the result in Fig. 1b, we assume that the width Δr of every belt has the same size of 0.3λ and the target plane is located in $z = 20\lambda$ in the simulation for removing the case of A in Fig. 1d. To obtain the unknown R_n of every belt, we solve its inverse problem described in Eq. (3) by using the trust-region dogleg Newton theory that is introduced in the Supplementary Materials [20]. The solved R_n is shown in the inset of Fig. 2b and their corresponding $\sin\alpha_n = [0.1387, 0.2576, 0.5643, 0.6638, 0.9548]$.

Conventionally, in order to obtain a supersmall focused spot, one always prefers to focus the light of high spatial frequency with large amplitude, which leads to a small size spot dominating at the target plane, and interfere the light from different spatial frequencies constructively, which enhances the focused spot. However, in superoscillatory focusing, we here show an abnormal phenomenon that the maximum amplitude ($|C_n|$) is located at the frequency with the intermediate value. This counterintuitive requirement for obtaining a small spot by superoscillation mainly depends on the fact that the superoscillation always oscillates with very small amplitude that can be considered as almost destructive interference [14]. The destructive interference in the superoscillation is also reflected by the phase of C_n that is shown in Fig. 2c. The phase difference between two neighboring belts in the designed zone plate is nearly π, which implies that the destructive interference is essentially required for realizing the superoscillation pattern in Fig. 2b. Thus, we can claim that the

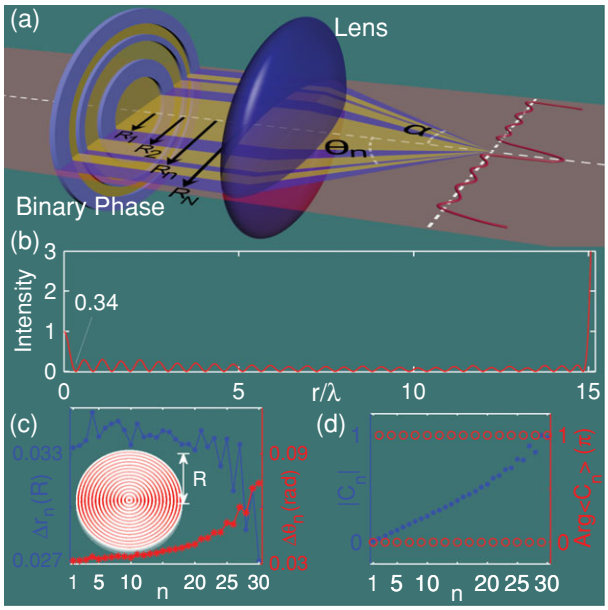

Figure 3 Generation of superoscillatory focusing with the sidelobe away from the center by using a binary phase and a lens. (a) The sketch of focusing a binary-phase modulated beam by a lens. The binary element has the phase of 0 and π, whose boundary is the circle with radius of R_n ($n = 1,2,\ldots,N$). The lens has an NA of $\sin\alpha$, where α is the maximum convergent angle. (b) A superoscillatory spot with size of 0.34λ and its sidelobe about 15λ away from the center by solving its inverse problem. Inset: 2-dimensional intensity profiles in the range $r \leq \lambda$. The specific radii of individual dielectric grooves are given in Supplementary Materials. (c) Width Δr_n (blue dot) of every belt and its corresponding angle width $\Delta\theta_n$ (red star) in the designed binary phase. Inset: 3-dimensional phase profile of this binary phase plate. (d) Modulus (solid circle) and phase (hollow circle) of amplitude-modulated coefficient C_n.

amplitude-modulated coefficient C_n has the alternating sign of $(-1)^n$ with its modulus small for low and high spatial frequency and large for the intermediate frequency, which is further confirmed by the case of focusing the light with rigorous single spatial frequencies (see Supplementary Materials). Nevertheless, this conclusion predicts that the zone plate is not ideal to realize a superoscillatory spot in Fig. 2b. Although the belt in the zone plate shows the excellent focusing property in a long range of R_n shown in Fig. 2e, the phase of C_n, that is the case of $r = 0$ in Fig. 2d, varies from 0 to 2π quasiperiodically with the increase of R_n. As a result, much effort must be made to obtain the phase difference of π for the alternating sign of C_n. Therefore, the zone plate may not be the best candidate to achieve a superoscillatory spot with its high sidelobe away, although we can use it to realize the superoscillatory spot in Fig. 2b.

Considering the difficulty of phase matching from a zone plate, we suggest another optical system containing a binary phase and a high numerical-aperture (NA) lens in Fig. 3a to realize the superoscillatory subwavelength focusing. The binary element with the phase 0 or π located in the entrance pupil of the focusing lens provides the phase difference of π for the generation of superoscillation in focusing [13, 21]. In the uniform illumination of an unpolarized beam, the electric field at the focal plane can be approximated by the Debye theory [22, 23]

$$\begin{aligned} U(r) &= \frac{2\pi i}{\lambda}\int_0^{\alpha} P(\theta)J_0(kr\sin\theta)\sin\theta\,\mathrm{d}\theta \\ &= \sum_{n=1}^{N}(-1)^n\frac{2\pi i}{\lambda}\int_{\theta_{n-1}}^{\theta_n}\sqrt{\cos\theta}\,J_0(kr\sin\theta)\sin\theta\,\mathrm{d}\theta \\ &= \sum_{n=1}^{N}(-1)^n U_n(r), \end{aligned} \tag{4}$$

where $P(\theta)$ is the apodization function that equals $p(\theta)\cdot\cos(\theta)^{1/2}$ for the lens obeying the sine condition [23, 24], $p(\theta)$ is the entrance pupil function that is $(-1)^n$ for the uniform illumination with the modulation of binary phase. The relationship between R_n and θ_n ($n = 0, 1, 2, \ldots, N$ with $\theta_0 = 0$, $\theta_N = \alpha$) is $R_n/f = \sin\theta_n$ for the sine lens used here, where f is the focal length of focusing lens. We define the amplitude modulation coefficient $C_n = (-1)^n U_n(0)$ and $A_n(r) = U_n(r)/U_n(0)$. Similarly, the inverse problem of constructing the superoscillation using the optical system in Fig. 3a can also be expressed by Eq. (3) with the unknown variable R_n (or $\sin\theta_n$). The amplitude modulation coefficient C_n with the alternating sign of $(-1)^n$ makes it easier to solve the inverse problem for generating the superoscillatory focusing. Figure 3b shows a constructed superoscillatory spot with a size of about $0.5r_R$ (0.34λ) and the high sidelobe about 15λ away from the center by using a 0.95 NA lens (see Supplementary Materials for the radius parameters).

This superoscillatory spot is obtained by padding 29 zero-intensity positions between the main spot and the sidelobe when solving its inverse problem with $N = 30$ variables. Compared with the result in Fig. 2b by using a zone plate, the spot in Fig. 3b almost keeps the same size, while the distance between its high sidelobe and center is nearly 10 times that in Fig. 2b, which mainly benefits from the binary phase (with a phase difference of π) for destructive interference. We can enlarge the distance further by padding more zero-intensity positions between the high sidelobe and the center. Figure 3c shows the structure of the designed binary phase by our method. The width Δr_n ($= R_n - R_{n-1}$) of belts in the binary phase tends to be diminishing at the outmost belts that are relative to the high spatial frequency. However, for a sine lens, the corresponding angle width $\Delta\theta_n$ ($= \theta_n - \theta_{n-1}$) of every belt is increasing so that the amplitude modulation $|C_n|$ shows the monotonically increasing tendency from the low spatial frequency to the high in Fig. 3d, which is different from the case in Fig. 2c. This is mainly attributed to the fact that every belt of binary phase corresponds to the spectrum (from $\sin\theta_{n-1}/\lambda$ to $\sin\theta_n/\lambda$) of spatial frequency not a quasisingle spatial frequency that occurs in zone plates. Through this example, we have shown that the method suggested here is valid to

solve the inverse problem of superoscillation by using the optical system in Fig. 3a.

Next, we discuss the method that distinguishes a superoscillatory spot in optical focusing. Although the superoscillatory spot has been widely investigated in optical focusing and imaging [9, 12, 15, 25], none provides a clear demonstration as to how small a spot has to be so that it can be considered as a superoscillatory spot. To our knowledge, the Rayleigh criterion ($r_R = 0.61\lambda/NA$) is mostly used to judge a superoscillatory spot in optical focusing [26]. However, it is a very rough method because there is no definition of superoscillation involved. In optics, a relevant and natural definition of superoscillation has been proposed by measuring the changing rate of the phase of a band-limited function in a local region [27, 28]. In particular, for the case of the 1-dimensional (or axisymmetric) band-limited function, i.e. the zone plate and a binary-phase-based lens, Berry and Dennis proposed a practical method for measuring the local wave number, $k(r) = \mathrm{Im}\{\partial_r[\ln F(r)]\}$, where $F(r)$ is the band-limited function [28]. Therefore, the definition of local wave number by Berry and Dennis is preferred in optical focusing. However, when we use Berry and Dennis's suggestion to evaluate the local wave number of a superoscillatory band-limited function in Fig. 4a, the calculated wave number in Fig. 4b is larger than the wave number of its maximum Fourier component only when the band-limited function has zero intensity. This means that, though the band-limited function indeed oscillates faster in the whole region $x \in [-0.8\lambda, 0.8\lambda]$ than its maximum Fourier component, Berry and Dennis's suggestion only predicts the superoscillation at the zero-intensity position. It is worth pointing out that Berry and Dennis's suggestion gives the wave number at a certain position but not in a region where Fig. 4b shows the large wave number only at the zero-intensity position. Therefore, in optical focusing, it is better to define the superoscillatory spot by measuring the phase-changing rate in a certain region.

In optical focusing, we constrain the definition of a superoscillatory spot on three conditions: 1) The optical system is axisymmetric so that a circular spot could be generated. 2) The superoscillatory spot must oscillate faster in a certain region of the target plane than its maximum Fourier frequency component. 3) "A certain region" is located at $r \le r_S$, where r_S is the first zero-intensity position of the electric field at the target plane by focusing the light only from the maximum Fourier frequency component. The reason for choosing the region $r \le r_S$ is to exclude the case shown by the black curve of Fig. 4c, which has the fast superoscillation at $r \ge r_S$ while its spot size is very large. In this region $r \le r_S$, the maximum Fourier frequency component only oscillates for one time without changing its phase, which is shown by the blue curve in Fig. 4c. If a spot oscillates faster in $r \le r_S$, this will lead to the generation of the intensity valley, where the high local wave number is located [28]. Thus, we can define a superoscillatory spot in optical focusing as: a spot is superoscillatory when its local wave number that is larger than the wave number of the maximum Fourier frequency is located in the region $r \le r_S$. In that case, a spot with its zero intensity

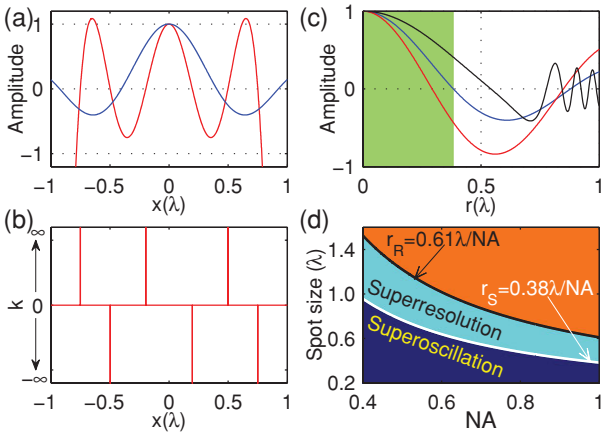

Figure 4 Superoscillatory criterion in optical focusing. (a) The amplitude profiles of a superoscillatory band-limited function with its zero-intensity position at $x = \pm 0.2\lambda$ (red) and its maximum spatial frequency component (blue). The band-limited function is the electric field at the focal plane by using the binary-phase-based 0.95NA lens in Fig. 3a with the solved $\sin\theta_n$ = [0, 0.3435, 0.6523, 0.8744, 0.95]. This superoscillatory band-limited function obviously oscillates faster in the region $x \in [-0.8\lambda, 0.8\lambda]$ than its maximum spatial frequency. (b) The local wave number of the band-limited function in (a) by using Berry's suggestion. (c) The amplitude profiles of various cases: the first zero-intensity position located in the colored region (red) and outside color region (black). The blue curve shows the amplitude of the maximum spatial frequency. (d) The spot size in different NA, which equals the sine ($\sin\alpha$) of the angle between the optical axis and the maximum convergent ray in free space. The two curves, which are the Rayleigh (black) and superoscillation (white) criterions, divide the focusing spot into three parts: subresolved (orange), superresolution (cyan) and superoscillation (dark blue).

located in $r \le r_S$ is superoscillatory, which is shown by red curves in Figs. 4a and c. This means that a superoscillatory spot has a smaller size than that (r_S) by only focusing its maximum spatial frequency, which implies that r_S can be taken as the superoscillatory criterion. When light with a single spatial frequency of $\sin\alpha/\lambda$ (α is the angle between the optical axis and the maximum convergent ray) is focused, its electric field at the target plane is proportional to the zero-order Bessel function $J_0(2\pi r \sin\alpha/\lambda)$ of the first kind, which gives $r_S = 0.38\lambda/\sin\alpha$. The superoscillatory criterion r_S has a similar shape to the Rayleigh criterion r_R. Figure 4d shows the spot size in different NA that is usually in terms of $\sin\alpha$ in free space. For a given NA, the spot in all the cyan and dark-blue areas below the Rayleigh criterion (black curve) can be called the superresolution spot and the spot in the dark-blue area below the superoscillation criterion (white curve) is the superoscillation spot, which means that the superoscillation spot is one subaggregate of the superresolution spot. The finely distinguished roadmap in Fig. 4d provides an instructive guide that the cyan area between the Rayleigh and superoscillation criterion is the best choice when one pursues a superresolution focusing spot without high sidelobe beyond the evanescent range. More

importantly, r_S implies a limitation of 0.38λ for the application of subwavelength spot without high sidelobe.

In summary, we have demonstrated a physical design roadmap of the superoscillatory focusing by using a zone plate or a binary-phase-based lens, with significantly enlarged field of view. The described inverse problem of superoscillation in terms of a nonlinear matrix equation enables construction of a customized superoscillatory pattern possible to be implemented without the traditional optimizing technique involved in the reported superoscillatory lens. This paves the way to a new scheme in further improving the resolution of the optical far-field imaging, and narrowing width of longitudinally polarized needle light for advanced data-storage performance [13]. In achieving a supersmall spot beyond the evanescent region, our result shows a counterintuitive phenomenon that the large spatial frequency with low intensity and destructive interference must be involved. Furthermore, the superoscillatory criterion proposed here gives us the direct insight into the spot pattern beyond the Rayleigh limitation, which sets a theoretical limitation of 0.38λ for the spot size in some applications that demand the narrow spot and low sidelobe simultaneously, i.e. optical lithography [29], high-intensity optical machining [30] and high-contrast superresolution imaging [31–33].

Acknowledgements. We thank Prof. Michael V. Berry for valuable discussions in defining a superoscillatory spot C.W.Q. acknowledges the support from National University of Singapore (Grant No. R-263-000-688-112).

Supporting information for this article is available free of charge under http://dx.doi.org/10.1002/lpor.201300123

Received: 14 August 2013, **Revised:** 11 October 2013, **Accepted:** 14 October 2013

Published online: 8 November 2013

Key words: Binary phase mask, Fresnel zone plate, superoscillation, subwavelength imaging, nanostructure.

References

[1] R. Dorn, S. Quabis, and G. Leuchs, Phys. Rev. Lett. **91**, 233901 (2003).
[2] N. Fang, H. Lee, C. Sun, and X. Zhang, Science **308**, 534–537 (2005).
[3] Z. Liu, H. Lee, Y. Xiong, C. Sun, and X. Zhang, Science **315**, 1686 (2007).
[4] W. Denk, J. H. Strickler, and W. W. Webb, Science **248**, 73–76 (1990).
[5] E. Betzig, G. Patterson, R. Sougrat, O. Lindwasser, S. Olenych, J. Bonifacino, M. Davidson, J. Lippincott-Schwartz, and H. Hess, Science **313**, 1642–1645 (2006).
[6] B. Huang, W. Wang, M. Bates, and X. Zhuang, Science **319**, 810–813 (2008).
[7] E. A. Ash and G. Nicholls, Nature **237**, 510–513 (1972).
[8] G. Binnig, H. Rohrer, C. Gerber, and E. Weibel, Appl. Phys. Lett. **40**, 178–180 (1982).
[9] E. T. F. Rogers, J. Lindberg, T. Roy, S. Savo, J. E. Chad, M. R. Dennis, and N. I. Zheludev, Nature Mater. **11**, 432–435 (2012).
[10] M. V. Berry and S. Popescu, J. Phys. A: Math. Theor. **39**, 6965–6977 (2006).
[11] P. J. S. G. Ferreira and A. Kempf, IEEE Trans. Signal Process. **54**, 3732–3740 (2006).
[12] F. M. Huang and N. Zheludev, Nano Lett. **9**, 1249–1254 (2009).
[13] H. F. Wang, L. P. Shi, B. Luk'yanchuk, C. Sheppard, and C. T. Chong, Nature Photon. **2**, 501–505 (2008).
[14] M.V. Berry, J. Phys. A: Math. Theor. **46**, 205203 (2013).
[15] F. M. Huang, N. Zheludev, Y. Chen, and F. Javier Garcia de Abajo, Appl. Phys. Lett. **90**, 091119 (2007).
[16] G. Toraldo di Francia, Nuovo Cimento **9**, 426 (1952).
[17] K. G. Makris and D. Psaltis, Opt. Lett. **36**, 4335 (2011).
[18] B. Born, and E. Wolf, Principles of Optics, 6th edn (Pergamon, Oxford, 1993).
[19] J. E. Dennis, and R. B. Schnabel, Numerical methods for unconstrained optimization and nonlinear equations (Prentice-Hall, Inc., New Jersey, 1983).
[20] J. Nocedal and S. J. Wright, Numerical Optimization, 2nd edn (Springer Series in Operations Research, Springer Verlag, New York, 2006).
[21] K. Huang, P. Shi, X. Kang, X. Zhang, and Y. Li, Opt. Lett. **35** 965–967 (2010).
[22] P. Debye, Ann. Phys. **335**, 57–136 (1909).
[23] Min Gu, Advanced Optical Imaging Theory, 75 (Springer-Verlag, New York, 1999).
[24] Q. Zhan, Adv. Opt. Photon. **1** (1), 1–57 (2009).
[25] F. M. Huang, T. S. Kao, V. A. Fedotov, Y. Chen, and N. I. Zheludev, Nano Lett. **8**, 2469–2472 (2008).
[26] E. Greenfield, R. Schley, I. Hurwitz, J. Nemirovsky, K.G. Makris, and M. Segev, Opt. Exp. **21**, 13425–13435 (2013).
[27] M. R. Dennis, A. C. Hamilton, and J. Courtial, Opt. Lett. **33**, 2976 (2008).
[28] M. V. Berry and M. R. Dennis, J. Phys. A: Math. Theor. **42**, 022003 (2009).
[29] H. Liu, B. Wang, L. Ke, J. Deng, C. C. Chum, S. L. Teo, L. Shen, S. A. Maier and J. Teng, Nano Lett. **12**, 1549–1554 (2012).
[30] M. Duocastella and C. B. Arnold, Laser Photon. Rev. **6**, 607–5621 (2012).
[31] H. Liu, B. Wang, L. Ke, J. Deng, C. C. Chum, S. L. Teo, L. Shen, S. A. Maier and J. Teng, Adv. Func. Mater. **22**, 3777–3783 (2012).
[32] C. Lu and R. H. Lipson, Laser Photon. Rev. **4**, 568–580 (2010).
[33] H. Wang, C. J. R. Sheppard, K. Ravi, S. T. Ho, and G. Vienne, Laser Photon. Rev. **6**, 354–392 (2012).

Optimization-free super-oscillatory lens using phase and amplitude masks

Kun Huang[1], Huapeng Ye[1], Jinghua Teng[2], Swee Ping Yeo[1], Boris Luk'yanchuk[3*], and Cheng-Wei Qiu[1*]

*Email: eleqc@nus.edu.sg; Tel: (65) 65162559; Fax: (65) 67791103

[1]Department of Electrical and Computer Engineering, National University of Singapore, 4 Engineering Drive 3, Singapore 117583, Singapore

[2]Institute of Materials Research and Engineering, Agency for Science, Technology and Research, Singapore 117602, Singapore

[3]Data Storage Institute, Agency for Science, Technology and Research, 5 Engineering Drive 1, Singapore 117608, Singapore

Supplementary Materials for Design Procedure and Criteria

1. The intensity and phase of light passing through a single belt with its radius r_0 and width Δr. In Fig. 1, we show the sketch of the diffraction of a belt with radius r_0 and width Δr. The angle between the ray emitting from the center of belt to the on-axis point at the target plane and the optical axis is α whose sine has the form of $\sin\alpha=r_0/(r_0^2+z^2)^{1/2}$. In order to evaluate the difference between the intensity profile of light passing through the transparent belt and the Bessel function $J_0(k_0 r\sin\alpha)$, we use the their root-mean-square error (RMSE)

$$RMSE = \sqrt{\frac{\sum_{n=1}^{N}\left\{A_n\left[r(n)\right]^2 - J_0\left[k_0 r(n)\sin\alpha\right]^2\right\}^2}{N-1}}, \qquad \text{(S1)}$$

where N is the number of sampling points in position r. If RMSE is small, the intensity profile at the target plane has a good approximation of the Bessel function. Figure 1(b) shows the dependence of the RMSE on the width Δr and radius r_0 (or $\sin\alpha$) of the belt when the propagating distance from the belt plane to the target plane is 20λ. We take N=300 in Fig. 1(b). We just display the cases for the RMSE smaller than 0.05, in which the good approximation can be obtained. In order to show the difference between the color and white region more straightforwardly, we select some positions, i.e. A in white region and B in color region, and plot their intensity profiles at the target plane in Fig. 1(d) and (e). When we choose the parameters $\Delta r = 1.7\lambda$ and $\sin\alpha=0.6$ at the position A in Fig. 1(b), the intensity profile has a bad approximation of Bessel function as shown in Fig. 1(d). However, for the position B with $\Delta r = 0.5\lambda$ and $\sin\alpha=0.6$, one can hardly distinguish between the intensity profile and Bessel function with its RMSE of 8.5×10^{-4} in Fig. S1(d). From Fig. 1(b), we can see the tendency that the approximation is good when the radius r_0 (or $\sin\alpha$) increases. For the belt with its width Δr smaller than the wavelength, its RMSE between the

intensity profile and Bessel function is also small enough to obtain a good approximation. If the width Δr increases, the better approximation happens at only the position in the feather-like region of Fig. 1(b). This implies that the careful weight in choosing the width of belt is required in designing a zone plate for super-resolution or super-oscillation focusing because the belt with its parameters located at the white region in Fig. 1(b) makes no sense in achieving a small spot. From this viewpoint, Figure 1(b) shows an instructive roadmap for designing a super-resolution or super-oscillation zone plate.

Interestingly, one can note that the white region in Fig. 1(b) always spreads to the position where $\Delta r = n\lambda$ (n=1, 2, …) and $\sin\alpha$=1. This phenomenon tells us a fact that light passing through the belt with the integer-wavelength width Δr and large radius r_0 has a destructive interference with the zero on-axis intensity at the center, which has no any improvement in reducing the spot size but contributing a large ring-like intensity. Therefore, for the belt with very large radius r_0, its width should be chosen as the value with integer wavelength when one pursues a small spot at the target plane.

Correspondingly, in Fig. 1(c), we show the modulated amplitude C_n with its intensity profile having a good approximation of Bessel function. According to the conclusion derived from Fig. 1(b), we just consider the color region with the width Δr smaller than the wavelength. In this region, for a belt with the fixed width Δr, its amplitude is large for the intermediate radius r_0 (or $\sin\alpha$) and small for the low and high radius r_0 (or $\sin\alpha$), which is well consistent with the amplitude requirement for super-oscillation focusing in Fig. 2(b). This shows the advantage for zone plate to realize the super-oscillatory focusing spot with its sidelobe away from the center.

To understand the properties of light passing through a single belt, we plot the phase and amplitude profiles for the cases of the belt with different radius r_0 and fixed width Δr=0.3λ in Fig. 2(d) and (e). The propagating distance is also chosen at z=20λ. The amplitude profile has the sharp variation for the small radius of the belt and the similar shape for the radius r_0 is larger than 40λ. However, the modulated amplitude $U(0)$ at r=0 has a peak near r_0=20λ and slowly decreases for the large radius r_0 of the belt. For its phase profile, there is a radial (along r) phase change of π where the zero intensity happens in Fig. 2(d). Moreover, the phase also changes with the increment of the radius of the belt, which means that the phase for every spatial frequency is different. One has to choose the suitable radius r_0 of belt to make the phase difference between the neighboring frequencies become π for realizing the super-oscillation focusing, which makes the zone plate behave badly in realizing a spot with sidelobe away from the center.

2. The trust-region Newton's theory for nonlinear equations

In this paper, the numerical solution for the nonlinear problem describing the inverse problem of super-oscillation by using a zone plate or a binary-phase modulated lens system is obtained by the well-developed trust-region Newton's theory, which is the most widely used algorithm for nonlinear equations. In this section, we just show the part that has the tight relationship with our case in the paper and ignore the proof, which can be found in the relative books for more details [S1, S2], for every theory used in our codes.

Newton' theory

For most nonlinear equations with multiple variables, the basic problem can be expressed as follows:

$$\text{Given } \Gamma\text{: } \mathbf{R}^n \rightarrow \mathbf{R}^n, \text{ find } \mathbf{x}^* \in \mathbf{R}^n \text{ such that } \Gamma(\mathbf{x}^*)=0 \tag{S2}$$

where Γ is assumed to be continuously differentiable. Here, in our cases, the function $\mathscr{F}$ has the form of $\Gamma(\mathbf{v})=L(r_m)+F(r_m)+\sum_n S(v_n,r_m)C(v_n)$ for the lens system and $\Gamma(\mathbf{v})= F(r_m)+\sum_n S(v_n,r_m)C(v_n)$ for the zone plate. For simplicity, we give the solution for the problem with one variable. We can

$$\Gamma(x_0 + p) = \Gamma(x_0) + \int_{x_0}^{x_0+p} J(t)dt\,, \tag{S3}$$

approximate the integral in Eq. (S3) by a linear term $J(x_0)\cdot p$, where $J(x_0)$ is the Jacobian of Γ(x). Therefore, Eq. (S3) can be simplified with

$$\Gamma(x_0 + p) = \Gamma(x_0) + J(x_0)p\,, \tag{S4}$$

Now, we can solve the step p that makes $\Gamma(x_0+p)=0$, which gives the Newton iteration for this problem. The solution is

$$\Gamma(x_0) = -J(x_0)p\,, \tag{S5}$$

$$x_1 = x_0 + p\,. \tag{S6}$$

From Eq. (S5) and (S6), one can see that the choice of step p is very important in solving the nonlinear problem successfully. Many methods has been developed to find the suitable step p for the various nonlinear problem. The trust-region method is the most popular one for its global convergence properties and rapid local convergence with exact solution.

Trust-region method

As shown in Eq. (S4), the step p is a root of the $\Gamma(x_0+p)=0$. Equivalently, the step p is also a minimum of the Euclidean norm $m(p)$

$$\begin{aligned} m(p) &= \frac{1}{2}\|\Gamma(x_k + p)\|_2^2 = \frac{1}{2}\|\Gamma(x_k) + J(x_k)p\|_2^2 \\ &= \frac{1}{2}\Gamma(x_k)^T\,\Gamma(x_k) + p^T J(x_k)^T \Gamma(x_k) + \frac{1}{2}\,p^T J(x_k)^T J(x_k)p \end{aligned}\,, \tag{S7}$$

where the sign $\|\cdot\|_2^2$ stands for the Euclidean norm and the s^T is the transpose of the matrix s. Hence, the subproblem of trust-region method is to find the minimum of function $m(p)$ in the limited region $\|p\| \le \Delta_k$, where Δ_k is the trust-region radius which has the positive value. Choosing the trust-region radius Δ_k at each iteration is the first problem that should be settled down in building the trust-region method. We follow the general way for evaluating the trust-region radius by the agreement between the model function $m(p)$ and the objective function $\Gamma(x_k)$ at the previous iterations. For the iteration with its step p_k, we can use the ratio

$$\rho_k = \frac{\|\Gamma(x_k)\|^2 - \|\Gamma(x_k + p_k)\|^2}{m_k(0) - m_k(p_k)}\,, \tag{S8}$$

where the numerator and denominator evaluate the actual and predicted reduction. Because the

step is obtained by minimizing the $m(p)$ over the region includes p=0, the denominator always has the nonnegative value. This implies that, if the ratio ρ_k is negative, the next objective value is larger than the current value $\Gamma(x_k)$. Moreover, when ρ_k is close to 1, it is the good agreement for this step, resulting that it is safe to use the trust region of this step in the next iteration. However, when ρ_k is very small (close to zero) or negative, we should decrease the radius of trust region. When we carry out this method in a computer code, its flowchart for the trust-region method has the form as Fig. S1.

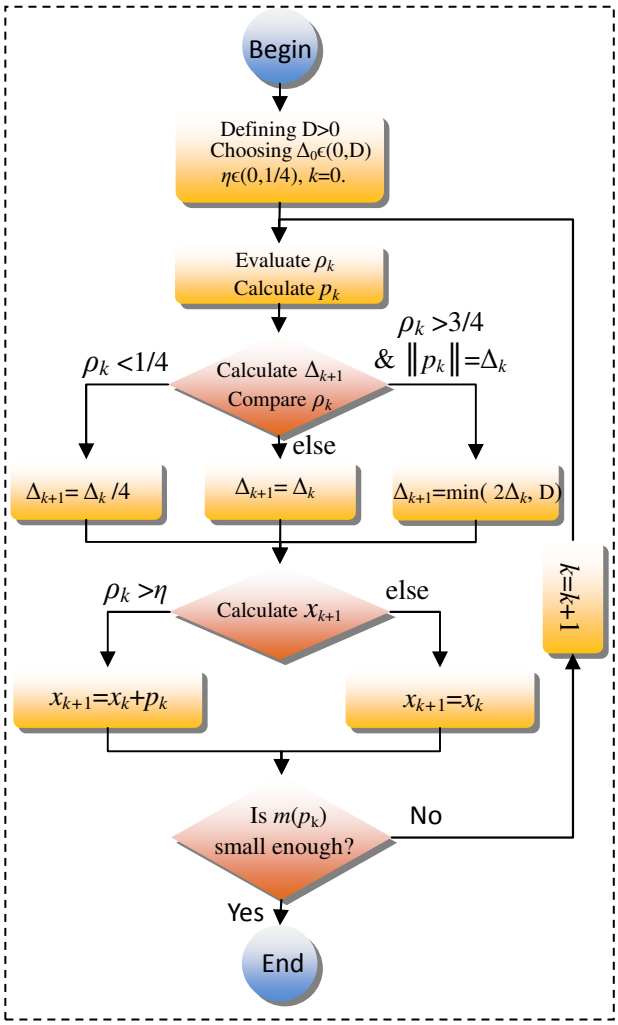

Figure S1 | The flowchart of the trust-region method based on the Newton's theory for non-linear equations.

In the flowchart, the calculation of p_k is usually carried out by using the dogleg algorithm, which is a quick and efficient method for p_k. Next, we introduce the dogleg algorithm.

Dogleg algorithm

To obtain the approximate solution p of min[$m(p)$] in Eq. (S7), we use the dogleg algorithm which is based on the Cauchy point p_k^C and the unconstrained minimizer p_k^J. The Cauchy point is used to quantify the sufficient reduction of p_k for global convergence proposes. The Cauchy point is

$$p_k^C = -\tau_k \left(\Delta_k \Big/ \left\| J_k^T \Gamma(x_k) \right\| \right) J_k^T \Gamma(x_k), \tag{S9}$$

where

$$\tau_k = \min\left\{1, \left\| J_k^T \Gamma(x_k) \right\|^3 \Big/ \left[\Delta_k \Gamma^T(x_k) J_k \left(J_k^T J_k \right) J_k^T \Gamma(x_k) \right] \right\}. \tag{S10}$$

To realize the curved trajectory needed in dogleg algorithm for quick convergence globally, the unconstrained minimizer p_k^J is introduced. When the Jacobian J_k has full rank, the $m_k(p)$ has the unique minimizer. Therefore, the unconstrained minimizer is the good approximation for obtaining the solution of min[$m(p)$]. The unconstrained minimizer has the form of

$$p_k^J = -J_k^{-1} \Gamma(x_k). \tag{S11}$$

In the practical implementation of dogleg algorithm, the Cauchy point and the unconstrained minimizer are combined together for determining the approximate solution p of min[$m(p)$]. The flowchart of dogleg algorithm is shown in Fig. (S2).

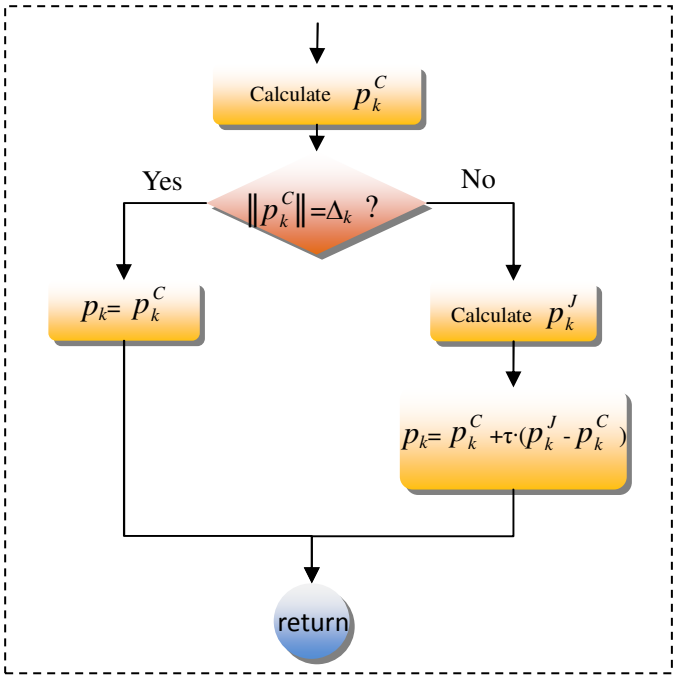

Figure S2 | The flowchart of dogleg algorithm for solving the subproblem in trust-region Newton method

3. Construct a super-oscillatory focused spot by focusing the light with rigorous single spatial frequencies

We have showed the generation of a super-oscillatory spot by using a zone plate and a binary-phase-base lens system. Here, to investigate the properties of the super-oscillatory focusing in optics, we construct an optical super-oscillatory pattern by interfering the light of different spatial frequencies with modulated amplitudes to display how the super-oscillation in optical focusing happens. For the focusing of a unpolarized beam with the single spatial frequencie, it can be approximated by the scalar Debye theory [S3, S4]. The electric field at the focal plane is proportional to

$$U(r,\theta)=\int_0^{2\pi}\exp(i\mathbf{k}\cdot\mathbf{r})d\varphi=\int_0^{2\pi}\exp[ik_0\sin\alpha\cdot r\cos(\varphi-\theta)]d\varphi=2\pi i\cdot J_0(k_0 r\sin\alpha), \quad \text{(S12)}$$

where $k_0=2\pi/\lambda$.Without loss of generality, we consider the interference of light with N different spatial frequencies whose amplitudes are modulated. Following the results in Eq. (S12), the total electric field after interference can be expressed as

$$f(r)=\sum_{n=1}^{N}C_n J_0(k_0 r v_n), \quad \text{(S13)}$$

where C_n and v_n are the modulated amplitude and the corresponding NA of n-th spatial frequency, respectively. First we show the simplest case of N=2 which is shown in Fig. S3(a). According to the results in Fig. 4, if the super-oscillation happens, the first zero-intensity position in the total electric field f after interference should be located at $r<r_s$. In Fig. S3(a), the first zero-intensity position is chosen at $r=r_0$. Then the zero intensity at $r=r_0$ can be realized by adjusting the amplitudes of f_1 and f_2. Here, we suggest a set solution of C_1=2.2041 and C_2=-1.2041, where the negative amplitude can be achieved by introducing a phase retardation of π in optics. The total electric field f seems to be the result that one pulls down the electric field f_1 of the maximum spatial frequency along the chromatic zone in Fig. S3(a) until the zero electric field (or completely destructive interference) occurs at r_0. When the pulling down of f_1 continues, the arbitrarily small super-oscillatory spot can be obtained only if the on-axis intensity at r=0 is nonzero, which gives the reason for the fact that it is possible to theoretically get a super-oscillatory spot with infinitesimal size [S5, S6]. Another consequence of pulling down f_1 is the further decrement of first valley with negative value that leads to the increment in intensity of high sidelobe as shown in Fig. S3(a), which can explain why the super-oscillation always accompanies with a high sidelobe [S5, S6]. From the case displayed in Fig. S3(a), we claim that, the super-oscillation in optics is the fact that the completely destructive interference happens at the some points with the neighboring interval smaller than the super-oscillation criterion r_s. The case in Fig. S3(a) shows the simplest prototype that represents the inverse problem of super-oscillation: what is the amplitude for every spatial frequency if one wants to realize the nonzero intensity at r=0 and the zero intensity at $r=r_0$ by using two given spatial frequencies.

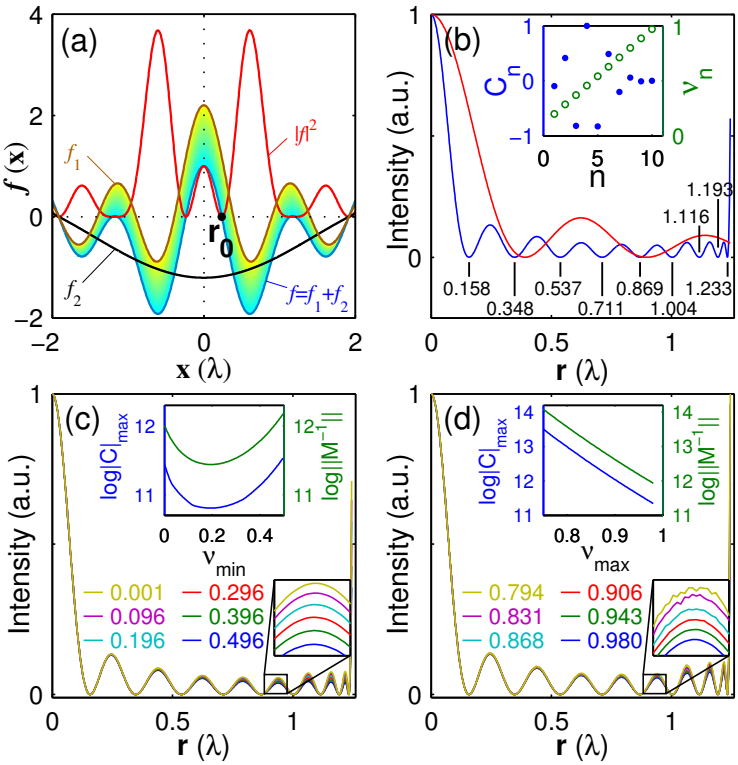

Figure S3 | The constructed optical pattern by inverse problem of super-oscillation. (a) The constructed super-oscillation by the light with two frequencies whose electric fields at the interfered area are f_1=2.041J_0(0.98k_0r)and f_2=-1.041J_0(0.2k_0r), respectively. **(b)** The intensity profiles of the constructed super-oscillation (blue) pattern by interference of the light with 10 spatial frequencies and the optical pattern (red) from the maximum frequency. Inset: the values of 10 given spatial frequencies (hollow circle) with equal interval and the solved **C** (solid dot) with the normalized value. **(c)** The intensity profiles of constructed super-oscillatory pattern when the minimum spatial frequency $v_{\min}$ is changing in the range of [0.001, 0.496] but the maximum spatial frequency $v_{\max}$ is fixed to 0.98. Inset: the maximum in the absolute value of the solved **C** (blue) and the corresponding norm $\|\mathbf{S}^{-1}\|$ (green) vs the different $v_{\min}$. **(d)** The intensity profiles of constructed super-oscillatory pattern when $v_{\max}$ is changing in the range of [0.75, 0.98] but $v_{\min}$ is fixed to 0.01. Inset: the maximum in the absolute value of the solved **C** (blue) and the corresponding norm $\|\mathbf{S}^{-1}\|$ (green) vs the different $v_{\max}$.

Next, we discuss the inverse problem of super-oscillation generally. Assuming that we want to realize the electric field $\mathbf{F}=[f_1,f_2,\ldots,f_M]^T$ at the prescribed position $\mathbf{r}=[r_1, r_2,\ldots, r_M]^T$ by using the interference of light from the given spatial frequencies $\mathbf{v}=[v_1, v_2,\ldots, v_N]^T$, the problem of determining the unknown amplitude $\mathbf{C}=[C_1,C_2,\ldots,C_N]^T$ can be expressed by

$$\mathbf{SC}=\mathbf{F}, \tag{S14}$$

where **S** is an M×N matrix that has its matrix element $S_{mn}=J_0(k_0r_mv_n)$ according to Eq. (S13). Because the only unknown variable in Eq. (S14) is **C**, it is a simple linear-equation problem to solve **C**, whose solution exists if N≥M. For simplicity, here we just discuss the case of N=M which implies that **S** is a square matrix. In this case, if **S** is invertible or has the nonzero determinate, which means the $\mathbf{S}^{-1}$ is not a singular matrix, **C** has the only solution of $\mathbf{C}=\mathbf{S}^{-1}\mathbf{F}$. For a

given $\mathbf{F}$, $\mathbf{S}^{-1}$ is the key parameter that determines the cost $\mathbf{C}$ for super-oscillation. Therefore, we can use the norm $\|\mathbf{S}^{-1}\|$ to evaluate the cost of super-oscillation. The norm $\|\mathbf{S}^{-1}\|$ depends on the prescribed position $\mathbf{r}$ and the spatial frequency $\mathbf{v}$. A fast super-ocillation means that the interval $\Delta r=r_{m+1}-r_m$ is very small. The m and m+1 row of $\mathbf{S}$ trends to have little difference so that $\mathbf{S}$ has its determinate $|\mathbf{S}|$ close to zero, which leads to the very large norm $\|\mathbf{S}^{-1}\|$ that causes a high cost in amplitude $\mathbf{C}$. Therefore, the faster super-oscillation always requires the higher cost.

Then, using the inverse problem of super-oscillation demonstrated above, we show an example that realizes a super-oscillatory spot with its high sidelobe away from center for super-resolution focusing. As shown in Fig. S3(b), for the N=10 given spatial frequencies $\mathbf{v}=[v_{\min}, v_{\min}+\Delta v,\ldots,v_{\min}+(\text{N-2})\cdot\Delta v, v_{\max}]$ with equal frequency interval $\Delta v=v_{\max}-v_{\min}/(\text{N-1})$ where $v_{\min}=0.201$ and $v_{\max}=0.98$, our aim is to use the frequencies $\mathbf{v}$ to realize a customized super-oscillatory pattern with its intensity profiles obeying $\mathbf{F}=[1, 0, \ldots, 0]^{\mathrm{T}}$ at the prescribed position $\mathbf{r}=[0, 0.158\lambda, 0.348\lambda,\ldots, 1.233\lambda]$. According to Eq. (S14), we can provide the solution $\mathbf{C}$ that is shown in the inset of Fig. S3(b). Using Eq. (S13) and the solved $\mathbf{C}$ by the inverse problem of super-oscillation, the intensity profile of constructed super-oscillatory pattern is displayed in Fig. S3(b). The constructed pattern indeed oscillates faster than the optical pattern from the maximum frequency. More importantly, the sidelobe in the constructed pattern is pushed several wavelengths away from the super-oscillatory main spot at the center by artificially padding the zero-intensity position between the sidelobe and main spot when setting the targeted $\mathbf{F}$ in practical application. In the intermediate area between the sidelobe and main spot, the zero intensity is used to suppress the high intensity of sidelobe so that the sidelobe has to move away from the center. The distance between the sidelobe and main spot can be enlarged by introducing more zero-intensity locations in their intermediate region, which implies more cost in the corresponding amplitude $\mathbf{C}$ [S7]. Nevertheless, this method provides an unrestricted route in theory for realizing a super-oscillatory focusing spot with its sidelobe arbitrarily far away from the center, which is a significant promotion in popularizing the super-oscillation in super-resolution imaging. Interestingly, the solved amplitude $\mathbf{C}$ has the alternating sign of positive or negative with its amplitude module small for low and high spatial frequencies and large for the intermediate spatial frequencies.

It is not the sole solution $\mathbf{C}$ for realizing the super-oscillatory pattern with the customized intensity $\mathbf{F}$ at the prescribed position $\mathbf{r}$ shown in Fig. S3(b) when we change the given spatial frequencies $\mathbf{v}$. In Fig. S3(c), we fix the maximum spatial frequency $v_{\max}/\lambda$ to be $0.98/\lambda$ and change $v_{\min}$ from 0.01 to 0.496, so that the N=10 given spatial frequencies have the form of $\mathbf{v}=[v_{\min}, v_{\min}+\Delta v,\ldots,v_{\min}+(\text{N-2})\cdot\Delta v, v_{\max}]$ with equal frequency interval $\Delta v=v_{\max}-v_{\min}/(\text{N-1})$ where $v_{\min}$ is changing and $v_{\max}=0.98$. According to the inverse problem described by Eq. (S14), we display the intensity profiles of some solutions in Fig. S3(c) that has absolutely the same intensity $\mathbf{F}$ at the prescribed position $\mathbf{r}$ although a little deviation between different frequency groups exists at the unprescribed position. It is worthy to note that both the norm $\|\mathbf{S}^{-1}\|$ and the maximum absolute value $|\mathbf{C}|_{\max}$ in every case experience a valley near $v_{\min}=0.2$ when $v_{\min}$ varies from 0.01 to 0.496. This reveals that the cost for every frequency group is different and an optimal solution is existent in our case, which is an undeniable proof that the optimization mechanism of super-oscillation is considerably developed by choosing the suitable spatial frequencies. The existence of the optimal solution for super-oscillation renovates the cognizance that there is no cheapest band-limited function for super-oscillation [S7]. Furthermore, we use the fixed $v_{\min}=0.01$ and varied $v_{\max}$ from

0.75 to 0.95 to generate the spatial frequency group **v** with equal frequency interval $\Delta v=v_{max}-v_{min}/(N-1)$. Likely, the customized intensity **F** at the prescribed position **r** is also achieved and shown in Fig. S3(d). In this case, the cost of super-oscillation exponentially decreases with the increment of v_{max}, which implies that the high spatial frequency is preferred in optimizing the super-oscillation with the smallest cost.

4. Parameters of binary phase mask in Fig. 3b

Table S1. Data of designed binary phase in Fig. 3b

n	$\sin\theta_n$	n	$\sin\theta_n$
0	0	16	0.5196
1	0.0317	17	0.5517
2	0.0635	18	0.5835
3	0.0955	19	0.6154
4	0.1291	20	0.647
5	0.1614	21	0.6796
6	0.1941	22	0.7113
7	0.2271	23	0.7435
8	0.2602	24	0.7742
9	0.2928	25	0.8063
10	0.3247	26	0.8357
11	0.3576	27	0.8676
12	0.3899	28	0.8949
13	0.4222	29	0.9244
14	0.4544	30	0.95
15	0.487		

References

[S1] Dennis, J.E. and Schnabel, R.B. Numerical methods for unconstrained optimization and nonlinear equations (Pretice-Hall, Inc, New Jersey, 1983).

[S2] Nocedal, J. and S. J. Wright. Numerical Optimization, Second Edition. (Springer Series in Operations Research, Springer Verlag, 2006).

[S3] Debye, P. "Der Lichtdruck auf Kugeln von beliebigem Material". *Annalen der Physik* **335**, 57-136(1909).

[S4] Min Gu, Advanced Optical Imaging Theory, 75 (Springer-Verlag, New York, 1999).

[S5] Rogers E. T. F., Lindberg J., Roy T., Savo S., Chad J. E., Dennis M. R., & Zheludev N. I., "A super-oscillatory lens optical microscope for subwavelength imaging." *Nature Mater.* **11**, 432-435 (2012).

[S6] Huang F. M. & Zheludev N. "Super-Resolution without Evanescent Waves." *Nano Lett.* **9**, 1249-1254 (2009).

[S7] Kempf. A. & Ferreira, P. J. S. G., S. "Unusual properties of superoscillating particles". *J. Phys. A* **37**, 12067-12076 (2004).